Al-Nahrain University, College of Engineering Journal (NUCEJ) Vol.19 No.2, 2016 pp.271 - 285

Fluidic Jet Vectoring at Subsonic Flow ay Using Counter Flow Method

Ali Abdul Almuhsen Al-Asady
Dep. of Mechanical Engineering
College of Engineering
Baghdad University
Email:dralicit@yahoo.com

Omar Hussien Ali
Dep. of Mechanical Engineering
College of Engineering
Baghdad University
Email:ohussienali@gmail.com

Abstract

Experimental & Computational and investigations of thrust vectoring by using counter flow method had been carried out in the present work. The experimental investigation included design and construction of test rig with rectangular duct with aspect ratio of (4.4) in order to investigate the effect of various geometric variables on thrust vectoring angle. Set of experiment at tests was carried out over the mass flow ratio ($\dot{M}s/\dot{M}p$) range $0 \leq (\dot{M}s/\dot{M}p) \leq 0.31$ with secondary slot gap height g/H= (0.0294, 0.0588, 0.088 and 0.1176) and coanda surface diameter R/H= (1.176, 2.353, 3.529and 4.705).

Load measurements were obtained using four load cells. The computational investigation involved a 3D numerical solution by FLUENT Software for some of experimental cases.

Experimental results show that the increase in secondary jet blowing rate lead to increasing in the jet vectoring angle, there are three zone can be observed, dead zone appears at low mass flow ratios, then followed by control region in which continuous thrust vector control can be achieved followed by a saturation region. The length of the dead zone' was also dependent on the size of the

Coanda surface diameter which a small diameter resulted in a prolonged 'dead zone' range, and the secondary gap height to the primary gap height had inverse relation with jet vectoring angle. The investigation shows that both the experimental and computational results obtained follow a similar trend line. Mach number is less than 0.5.

Keywords: Thrust vectoring angle; Jet vectoring; Coanda Effect; counter flow; mass flow ratio.

1. Introduction

The maneuverability of aircraft is traditionally achieved by the use of aerodynamic control surfaces such as ailerons, rudders, elevators and canards. The deflection of these surfaces modifies the exterior shape of the vehicle in critical points of its structure, thus creating changes in the aerodynamic forces and moments acting on the vehicle and causing it to maneuver, such traditional methods are heavy, complex and need continuous maintenance [2].

The development of another source of control became necessary, especially for high performance aircraft, whose survivability in combat depends mostly on their ability to maneuver. An alternative to such classical methods is thrust vector control which has successfully been identified and demonstrated many potential benefits to high-performance aircraft .thrust vector control (TVC) helps to improve the flying qualities, thus extending the flight envelope to regions of speed/angle of attack that could not be reached by the use of aerodynamic control alone. Flights using TV nozzles instead of traditional nozzles can reduce or eliminate the need for horizontal and vertical tails. The advantages of achieving separation on the rear tail are reduced aircraft weight and better stealth than other conventional aircrafts. Moreover, the cost of the maintenance of the tail is also reduced. It provides the potential for a vertical component of thrust which may be used, especially at low speeds, to augment the lift force generated by the wings. This allows the aircraft to take off in a shorter distance, and ascend at a higher rate. During landing, vectored thrust can be used to supplement the lift force generated by the wings, and approach speeds may be reduced without changing the rate of descent. The benefits of short takeoff and landing aircraft are especially attractive for landing on aircraft carriers or on damaged airfields. Traditionally the wings are the sole mechanism for generating lift. However they have aerodynamic limitations, namely airfoil stall, which causes a dramatic decrease in airfoil performance and must be avoided to maintain adequate control of the aircraft. Thrust vectoring can be used to maintain or re-establish control under stalled conditions, thus enhancing the overall maneuverability of the plane. In missile applications, multi axis thrust vector control could be employed for steering control at potentially considerably lower expense in terms of vehicle weight and cost [7].

In free surroundings, a jet of fluid entrains and mixes with its surroundings as it flows away from a nozzle. When a surface is brought close to the jet, this restricts the entrainment in that region. As flow accelerates to try balance the momentum transfer, a pressure difference across the jet

results and the jet is deflected closer to the surface - eventually attaching to it. Even if the surface is curved away from the initial direction, the jet tends to remain attached. This effect can be used to change the jet direction. In doing so, the rate at which the jet mixes is often significantly increased compared with that of an equivalent free jet [9].

Fluidic thrust vectoring system relies on a phenomenon known as Coanda effect. It states that fluid and gases jets have a natural tendency to attach to the wall, which is projected close to them and follow the convex curvature of the solid boundary. The principle was named after Romanian aerodynamicist inventor Henri-Marie Coanda, 1930, who was the first to understand the practical importance of the phenomenon for aircraft development. In order to describe this phenomenon, the tangential jet sheet which exits over the curved surface is supposed. This curvature can turn through a full 180° or more.

The jet remains attached to that curved surface because of a balance between the sub ambient pressure in the jet sheet and the centrifugal force in the jet going around the curvature. Initially, at very low blowing values, the jet entrains the boundary layer to prevent after flow separation and is thus a very effective boundary layer control

Eventually, as the jet continues to turn, a rise in the static pressure plus viscous shear stress and centrifugal force combine to separate the jet sheet and a new stagnation point and stagnation streamline are formed on the trailing edge parameters that affect the ability for flow to remain attached to the curved surface include the free stream velocity, radius of curvature and slot size and blowing pressure [1].

There are various methods to direct the exhaust thrust of a jet engine or missile system.

The conventional methods, which rely on mechanical means and the most recent methods, which are fluidic-based thrust vectoring techniques. In1960s, the idea of using gimbals and swivel mechanism for the non-axisymmetric nozzle was introduced. First generation thrust vectoring nozzles consisted of movable vanes that, through mechanical actuators, deflected the engine's exhaust.

The thrust vectoring nozzles that are use mechanical actuators. The addition of hydraulic mechanical actuators is a penalty to the aircraft's gross weight. Such mechanisms are to operate on the high temperature exhaust gases, thus requiring sophisticated cooling systems and/or the use of temperature resisting materials. For this reason, the manufacturing and operation costs are also expected to increase. Furthermore, a fundamental aspect in any control system must also be considered: the dynamic response. When mechanical actuators are used, the response of the jet is limited by the response of the actuator.

Owing to the disadvantage of MTV, researchers want to investigate novel methods to achieve the same TV capabilities without using external moving parts. FTV, as an alternative method, has been investigated since 1990 [6].Instead of deflecting mechanical parts to create vectored thrust, an FTV nozzle uses In this case, one or more secondary airstreams are used to redirect the primary jet, thus achieving thrust vectoring without movable parts. The main advantages of this type of technology are: the elimination of movable parts, simplifying the hardware, reducing weight and cutting maintenance needs; and the fast dynamic response inherent to fluidic devices and can be provide effective flow deflection as well as eliminate the problems associated with additional mechanical parts. Such fluidic techniques are expected to, when compared with the mechanical schemes, reduce nozzle weight up to 80% and maintenance costs up to 50 % [3].

There are six different FTV methods: co-flow FTV, counter-flow FTV, shock vector control FTV, throat shifting FTV, combined vectoring methods and synthetic jet actuator. All these methods use secondary jet flows for TV. Each method has been investigated both experimentally and numerically with different levels of success.

The higher entrainment rates of a counter flowing shear layer lead to the idea of using it to control the direction of a jet, see **Fig. 1.** This concept, called counter flow thrust vectoring (CFTV), was proposed by [9]. Jet deflection is achieved by fitting the jet's nozzle with a collar (Conda surface) leaving a small gap between them. Instead of injecting secondary stream of air, Suction is applied to this gap, to create counter flow secondary stream in the confined region between the jet and the collar [5].The basic geometry of a CFTV nozzle is illustrated in**, Fig 2**

2. Numerical Simulation

Numerical simulations allow the analysis of a complex phenomenon without resorting to expensive prototype and difficult experimental measurements. In order to analyze the flow field at the exit of primary and secondary duct, a solution of **Navier-stokes** equations and $\mathbf{k-\epsilon}$ turbulence model equations are required.

In the present work, the mathematical model of the problem was solved numerically using a **CFD Code FLUENT 6.3.26** after describing the mesh model using the Gambit 2.2.30. The geometry is generated by using GAMBIT 2.2.30 as three regions of interest. The effects of Coanda surface geometry and secondary gap height on vectoring angle for increasing secondary jet blowing rates were investigated. The CFD simulations provided

force data which were then compared to the experimental data obtained.

2.1. Governing Equations

Conservation equations for continuity and momentum for turbulent model of the flow are presented in FLUENT built – in solver. It is important here to refer back and discuss the general conservations equations as follows:

2.1.1 The Mass Conservation (Continuity) Equation

The equation for conservation of mass, or continuity equation, can be written as follows;

$$\frac{\partial \rho}{\partial t} + \nabla.(\rho\, \vec{v}) = 0 \quad \text{.... (1)}$$

Where:

$\vec{v}$: is the velocity vector.

For incompressible flow (ρ=constant) and the equation above is simplified to be:

$$\nabla.\vec{v} = 0 \quad \text{.... (2)}$$

2.1.2 Momentum Conservation Equations

Conservation of momentum is described by:

$$\frac{\bar{u}\partial\bar{u}}{\partial x} + \frac{\bar{v}\partial\bar{u}}{\partial y} + \frac{\bar{w}\partial\bar{u}}{\partial z} = -\frac{1}{\rho}\frac{\partial\bar{p}}{\partial x} + \nu(\nabla^2\bar{u}) - \frac{\partial\overline{(\grave{u})^2}}{\partial x} - \frac{\partial\overline{(\grave{u}\grave{v})}}{\partial y} - \frac{\partial\overline{(\grave{u}\grave{w})}}{\partial z} \quad \text{.... (3)}$$

$$\frac{\bar{u}\partial\bar{v}}{\partial x} + \frac{\bar{v}\partial\bar{v}}{\partial y} + \frac{\bar{w}\partial\bar{v}}{\partial z} = -\frac{1}{\rho}\frac{\partial\bar{p}}{\partial y} + \nu(\nabla^2\bar{v}) - \frac{\partial\overline{(\grave{u}\grave{v})}}{\partial x} - \frac{\partial\overline{(\grave{v})^2}}{\partial y} - \frac{\partial\overline{(\grave{v}\grave{w})}}{\partial z} \quad \text{.... (4)}$$

$$\frac{\bar{u}\partial\bar{w}}{\partial x} + \frac{\bar{v}\partial\bar{w}}{\partial y} + \frac{\bar{w}\partial\bar{w}}{\partial z} = -\frac{1}{\rho}\frac{\partial\bar{p}}{\partial z} + \nu(\nabla^2\bar{w}) - \frac{\partial\overline{(\grave{u}\grave{w})}}{\partial x} - \frac{\partial\overline{(\grave{w}\grave{v})}}{\partial y} - \frac{\partial\overline{(\grave{w})^2}}{\partial z}. \quad \text{.... (5)}$$

Where:

$$\nabla^2 = \frac{\partial^2}{\partial x^2} + \frac{\partial^2}{\partial y^2} + \frac{\partial^2}{\partial z^2} \quad \text{.... (6)}$$

2.1.3 $K-\epsilon$ Equation

The $\mathbf{k-\epsilon}$ turbulence model equation is written as:

$$\frac{\partial}{\partial t}(\rho k) + \frac{\partial}{\partial x_i}(\rho k u_i) = \frac{\partial}{\partial x_j}\left[\left(\mu + \frac{\mu_t}{\sigma_k}\right)\frac{\partial k}{\partial x_j}\right] + P_k + P_b - \rho\epsilon - Y_M + S_k \quad \text{.... (7)}$$

2.2 Definition of Boundary Conditions

In the three dimensional case a correct definition of boundary conditions is even more difficult than in the two dimensional case. In the present work, the boundary conditions specified in the calculations are:

1. The solid wall boundary condition represents an impermeable boundary and its mathematical formulation is relatively simple, the normal component of velocity is zero.
2. Symmetry boundary conditions are used when the physical geometry of interest and the expected pattern of the flow have mirror symmetry. They can also be used to model zero-shear slip walls in viscous flows.
3. Inlet boundary: the inflow velocity (primary flow velocity).
4. Outlet boundary: outlet pressure and the secondary flow velocity. See **Fig .3.**

3. Experimental Work:

A schematic drawing of the experimental set-up is shown in **Fig .4.** An experimental rig was designed and constructed in the Heat Transfer Lab, at the Mechanical Engineering Department, University of Baghdad .the test section used in the present study Consists of rectangular duct. The main dimensions of the duct are the width W=75 mm, height of H=17 mm and length of L= 750 mm. This duct was made of aluminum, utilizing different compatible secondary Coanda surfaces.

A total of four flaps with different configurations were examined in order to investigate the effects of varying collar diameter R =20 mm, 40 mm, 60 mm and 80mm (R/H= 1.176, 2.353, 3.529 and 4.705) into the thrust-vectoring angle**.** These flaps were made of aluminum with length of 15mm and box with four air intake openings to pull a uniform flow from the secondary slot gap height. Furthermore, four different secondary slot gap heights g = 0.5 mm, 1 mm, 1.5 mm and 2 mm (g/H= 0.0294, 0.0588. 0.088, 0.1176), and fifteen different secondary air mass flows were tested for each flap with a main jet speed at 15m/s and 18 m/s . By positioning the Coanda surface at the exit of the primary nozzle and introducing the secondary stream of counter - flowing air, parallel to the Coanda surface, counter-flow fluidic thrust vectoring can be obtained. The centrifugal blower with flow rate $11^{m^3}/_{min}$, maximum velocity 25 m/s and pressure at 1.1 bars is suitable to provide the main jet with 15m/s and18 m/s. The ejector was selected to provide the secondary jet. The load cells were selected to be capable to hold the test section without any damage to load cell circuit and have the sensitivity to measure the reaction. flow meter with a range from (0.0225 to 0.45) $^{m^3}/_{min}$ measure The volumetric flow rate of the secondary air passing through the pipes from the secondary slot gap height to ejector, also A vane anemometer which used in the present study to measure air velocity in the primary flow . The thrust vectoring angle obtained by eq. (8)

$$\delta v = \tan^{-1}\left(\frac{RY}{Rx + \dot{M}s\, Vs + \dot{M}p\, Vp}\right) \quad \text{.... (8)}$$

4. Results and Discussion:

4.1. Experimental Results and Discussion:

A systematic series of tests were carried out in order to investigate the effect of various geometry variables and flow condition on thrust vectoring angle. These included the secondary gap height (g), Coanda surface diameter (R) and the mass flow ratio (Ṁs/Ṁp).

4.1.1. Varying Secondary Gap Height (g/H):

Fig.5 shows the relationship between the mass flow ratio Ṁs/Ṁp (secondary flow rate/ primary flow rate) and the resulting thrust vector angle for various secondary gap heights at a constant Coanda surface diameter of R/*H* = 1.176. Four different secondary gap heights were tested of g/H= (0.0294, 0.0588. 0.088, 0.1176). The results show that as the secondary jet blowing rate is increased, the thrust vector angle value increased to maximum value equal to 33.1 degree. The reason for this behavior is: as the amount of suction applied increases two balancing effects take place at the same time: the gap pressure decreases resulting in higher secondary flow velocity, and the jet deflects towards the collar causing a decrease in the secondary flow area.

It can be seen that as the secondary gap height value increased, the values obtained for vectoring angle decrease from maximum value (33.1) degree for g/H = 0.0294 to maximum value (24.1) degree for g/H =0.1176 accordingly at each mass flow ratio tested with the velocity of primary flow equal to Vp=18m/s.

Figs. (6–8) show the relation between Ṁs/Ṁp and thrust vector angle of the tests at constant coanda surface diameter of R/H= (*2.35*, 3.53and 4.705) respectively. The results show that as the secondary jet blowing rate is increased, as the thrust vector angle value increased. It can be seen that as the secondary gap height increases, the values obtained for vectoring angle decrease accordingly at each mass flow ratio tested.

gap height is a very important parameter in the CFTV nozzle. A compromise for secondary gap height must be found for each application because: on the one hand, large gaps lead to increasing secondary flow values and the collar is not too close to the nozzle, this means that the collar is not located in the area from which the jet is entraining; therefore it does not "feel" its presence.

On the other hand, small gaps will assist attachment, because the jet is closer to the collar wall, when the collar is closer to the nozzle, it will come to a certain distance where it will restrain the natural jet entrainment, because the jet has its surrounding area blocked by the presence of the collar. And smaller values of δv will be enough for jet impingement. also The small gap height lead to smaller cross section area for secondary duct which affect the velocity value at the coanda surface for the same amount of primary flow rate.

A high velocity value produces a low pressure region which is responsible for vectoring the primary jet. The influence of gap height will therefore be felt in both attachment occurrence and secondary flow requirements.

The results shows that at very low secondary jet blowing rates i.e. **Ṁs << Ṁp**, the thrust vector angle is very small and there appears to be a 'dead zone' in which no flow control can be achieved. This phenomenon can be attributed to the fact that the Coanda effect cannot function at low secondary jet blowing rates.

At low secondary jet blowing rates, the secondary jet separates early from the Coanda surface. In extreme cases, control reversal can occur (negative vectoring angle) whereby the primary jet vectors in the opposite direction before vectoring in the direction expected. In this instance, the faster moving primary jet entrains the slower moving air of the secondary jet and instead of adhering to the Coanda surface and remaining attached far downstream, the secondary jet separates and a high pressure region forms.

The entrainment air has the effect of skewing the primary jet velocity distribution towards the opposite Coanda surface and the differential pressure gradient created vectors the primary jet in that direction due to the high pressure region.

After the 'dead zone', the Coanda effect dominates and the curve enters a region in which a large increase in thrust vector angle can be achieved for relatively small increases in the secondary jet blowing rate. In this region that continuous control of the primary jet can be achieved. From now on the thrust vector angle, and hence the thrust vector force generated, will enter a hypothetical region of saturation i.e. the thrust vector angle reaches an almost constant value, for any increase in secondary jet blowing rate. As shown in figures **Figs.(5-8)** the experimental results followed a similar trend. This is shown schematically in **Fig. 9**.

4.1.2. Varying Coanda Surface Diameter (R/H):

Fig. 10 shows the relationship between the mass flow ratio Ṁs/Ṁp and the resulting thrust vectoring angle for various Coanda surface diameters at a constant secondary gap height ratio of g/H = 0.0294. Four different coanda surface diameters cases were tested in the range R/H= (1.176, 2.353, 3.529 and 4.705). As shown in **Fig.10**, the results show that as the secondary jet blowing rate is increased, the thrust vector angle value increases. It can be seen that as the conda surface diameters increased, the values obtained

for vectoring angle increase accordingly at each mass flow ratio tested.

The reason for this relation is clear. Increasing collar length increases the area on which the gage collar pressure distribution -ΔPC can act. Since the level of-ΔP exit is indicative of the overall gage collar pressure distribution , the resultant normal collar force Fcy is increased proportionally greater for a longer collar at a fixed -ΔP exit, the increase in normal collar force results in larger thrust vector angles .

Also the Coanda surface diameter is increased the gradient of the curve becomes steeper once the 'dead zone' has been overcome. The diameter of the Coanda surface also determines the size of the 'dead zone' and hence where the onset of the control region begins. The results show that the secondary jet is more likely to separate from a Coanda surface with a small diameter and as a consequence the 'dead zone' will be prolonged over a wider range of secondary jet blowing rate values, because the large diameters provide as larger surface that fluid will attach to it. **Figs .(11-13)** show the relation between Ṁs/Ṁp and thrust vectoring angle of the tests at constant gap height of g/H= (0.0294 .0588, 0.088 and 0.1176) respectively. Four Coanda surface diameters were tested R/H= (1.176, 2.353, 3.529 and 4.705) and the result follow the same behavior as, **Fig. 10.**

4.2 Numerical Results:

Seven cases have been studied. Four different varying secondary gap height at constant coanda surface(R/H) =4.705 and four varying conda diameter with constant secondary gap height (g/H)=0.05882. The results directly reported from FLUENT for the resolved RY and Rx forces on the coanda and ducts walls to obtain the jet vectoring angle. **Fig.14.** Show a velocity contour at R/H=1.176, g/H= 0.0588 and Ṁs/Ṁp =14.74%.

4.2.1. Varying Secondary Gap Height (g/H):

Fig.15. Shows the relationship between thrust vector angle and the mass flow ratio for various secondary gap heights at constant Coanda surface diameter of R/H =4.705. Four different secondary gap heights were tested in the range of g/H= (0.0294, 0.0588. 0.08823 and 0.1176). the result show that as the secondary jet blowing rate is increased, the thrust vector angle increases and as the secondary gap height increases, the values obtained for vectoring angle decrease accordingly at each mass flow ratio tested.

4.2.2VaryingCoandaSurface Diameter (R/H):

Fig .16.shows the relationship between thrust vectoring angle and the mass flow ratio (Ṁs/Ṁp) for various Coanda surface diameters at constant secondary gap height ratio of g/H = 0.0588. four different Coanda surface diameters were tested in the range of g/H= (1.176, 2.353, 3.529 and 4.705).the result show that as the secondary jet blowing rate is increased, the thrust vector angle increases and as conda surface diameter increases, the values obtained for vectoring angle increase6 accordingly at each mass flow ratio tested.

4.3 Smoke Flow Visualisation:

Fig .17.shows the visualisation of a non-vectored primary jet (Vs = 0 Ṁs/Ṁp = 0). **Fig .18.**Visualisation of a vectored primary jet for Coanda surface diameters in the range of R/H= 3.529 and Ṁs/Ṁp =0.2613 at constant secondary gap height ratio of g/H = 0.0588.

4.4. Verification:

The experimental and numerical results for Vp=18 m/s has been compared with each other, as shown in **Figs. 19& 20.** Figure reveals that the numerical follows the same behavior as the present experimental results but is approximately with a mean of difference of 9.6% and 12.2% respectively between max thrust vector angle.

However, the extent of the 'dead zone' for the experimental work is more prolonged than that obtained in the theoretical work. The computational work has also highlighted both the control and saturation regions as seen previously in the experimental results. At low secondary jet blowing rates, the CFD investigation predicted greater thrust vectoring angle than those obtained during the experimental tests for approximately the same mass flow ratio. To verify the results obtained from the present study, a comparison was made with the results achieved by previous studies. The present results Thrust vectoring angle for varying secondary gap height at constant Coanda surface diameter **Figs. (5-8)** agree with the results of (the experimental and theoretical work) [8], shown in **Fig.21,** and with (the experimental and numerical work) [4] ,shown **Fig .22.** The present results Thrust vectoring angle for varying Coanda surface diameter at constant secondary gap height shown in **Figs. (10-13)** agrees with the results of [4] ,the experimental and numerical work shown in **Fig23.**

5. Conclusions:

Both the experimental and computational results obtained followed a similar trend line. A 'dead zone' appears at low secondary jet mass flow rates. There then follows a control region in which continuous thrust vector control can be achieved followed by a hypothetical saturation region in which the thrust vector coefficient will reach an almost constant value, for any increase in secondary jet blowing rate. The length of the 'dead zone' was also dependent on the size of the Coanda surface diameter. A small diameter resulted in a prolonged 'dead zone' range. The thrust vector angle is dependent on the Coanda

surface diameter and the mass flow ratio. Thrust vectoring angle increased by increasing mass flow ratio Ṁs/Ṁp and Coanda surface diameter, once the dead zone has been overcome and decreasing the secondary slot gap height.

References:

[1] Banazadeh, A.; Saghafi, F.; Ghoreyshi, M. and Pilidis "Experimental and computational investigation into the use of co-flow fluidic thrust vectoring on a small gas turbine," The Aeronautical Journal.pp.17-25, 2008.

[2] Collins, Emmanuel G., Jr "Feedback Control Design for Counter flow Thrust Vectoring," American Control Conference .pp.3654 -3659, 2005.

[3] Deere K.A "Summary of Fluidic Thrust Vectoring Research Conducted at NASA Langley Research Center," American Institute of Aeronautics and Astronautics. Vol. 2003 issue 3800, 2003.

[4] Mason, M.S. and Crowther, W.J "Fluidic Thrust vectoring of Low Observable Aircraft," CEAS Aerospace Aerodynamic Research Conference.pp.13/39, 2002.

[5] Maria Madruga Santos "Experimental Study on Counter Flow Thrust Vectoring of a Gas Turbine Engine," Electronic Theses, Treatises and Dissertations. Paper 2080 , 2004.

[6] Muroran institute of Technology Aerospace Engineering Division "Numerical and Experimental Studies of Fluidic Thrust Vectoring Mechanisms," Doctoral Dissertation, 2011.

[7] Strykowski, P.J.Vectoring "Thrust using Confined Shear Layers," Naval Research reviews .vol.51 (3, 4), 1999.

[8] Van der Veer and Paul J. Strykowski "Thrust Vector Control of Rectangular Jets using Counter Flow Method," report document to AIR FORCE OFFICE of SCIENTIFIC.PP.20332-0001, 1995.

[9] www.thermofluids.co.uk/effect.php.

Nomenclature:

Symbol	Definition	Units
H	Height of Primary Jet	mm
g	Gap height of Secondary Jet	mm
k	the turbulent kinetic energy	
L	length of Primary Jet	mm
Ṁp	Primary Mass Flow Rate	Kg/s
Ṁs	Secondary Mass Flow Rate	Kg/s
P_b	The generation of turbulence kinetic energy due to buoyancy.	
P_k	The generation of turbulence kinetic energy due to the mean velocity gradients	
S	the modulus of the mean rate-of-strain tensor	
R	Coanda Surface Diameter	mm
Rx	Horizontal Force	kg
Ry	Vertical Force	kg
Vp	velocity of primary flow	m/s
Vs	velocity of secondary flow	m/s
$\bar{u}$	Average Velocity in x Axes	m/s
$\grave{u}$	Fluctuations Velocity in x Axes	
$\bar{v}$	Average Velocity in y Axes	m/s
$\grave{v}$	Fluctuations Velocity in y Axes	
W	Width of Primary Jet	mm
$\bar{w}$	Average Velocity in z Axes	m/s
$\grave{w}$	Fluctuations Velocity in z Axes	
δ	Thrust Vectoring Angle	degree
ρ	Density	kg/m^3
μ_t	the turbulent viscosity	
3-D	Three Dimension	
CFD	Computational Fluid Dynamics	
CFTV	Counter flow thrust vectoring	
FTV	Fluidic thrust vectoring	
MTV	Mechanical thrust vectoring	

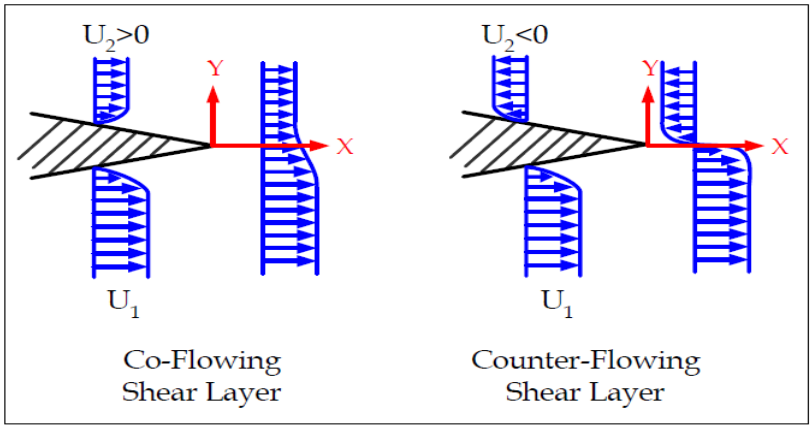

Figure 1: Schematic of Co flowing and counter Flowing shear layers.

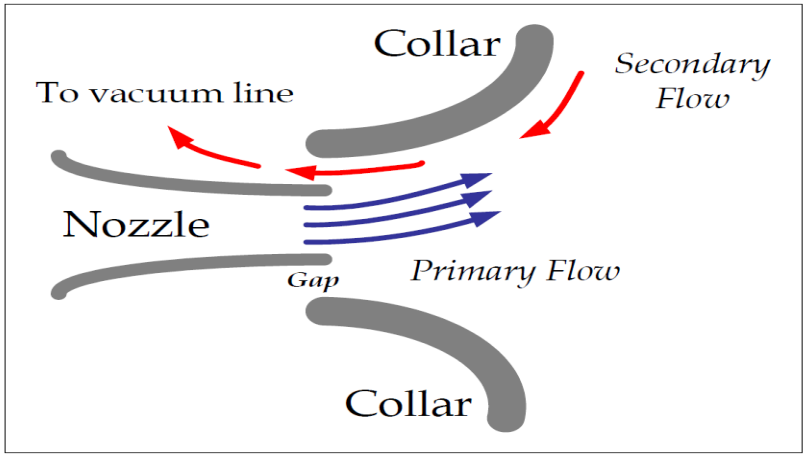

Figure 2: Schematic of Counter Flow Thrust Vector Control (CF-TVC) geometry.

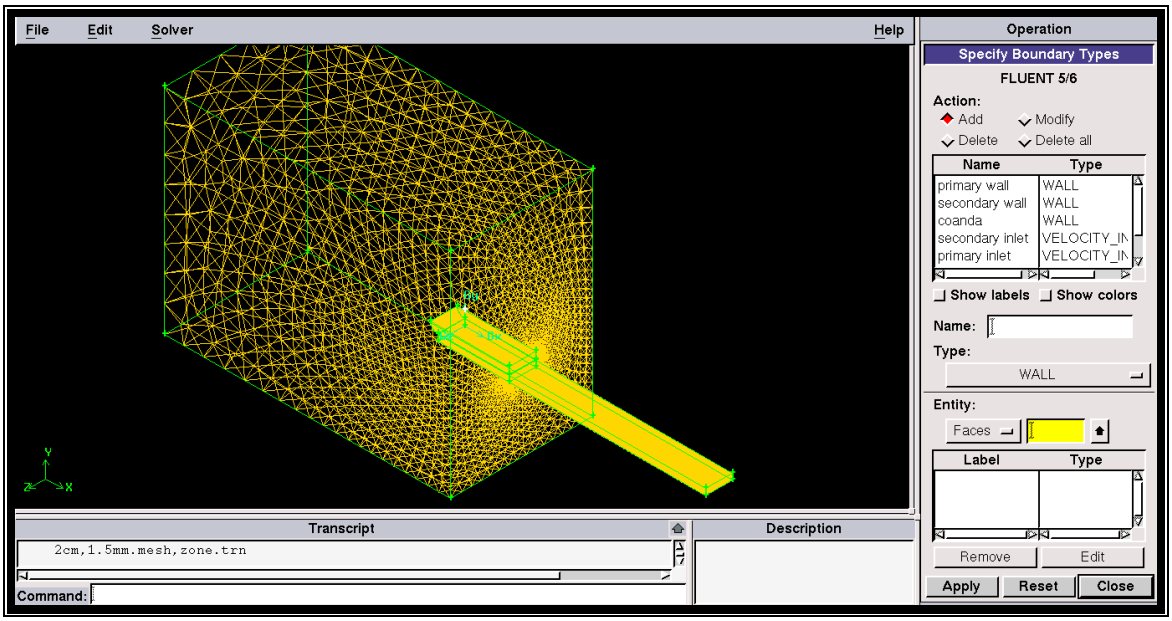

(A)

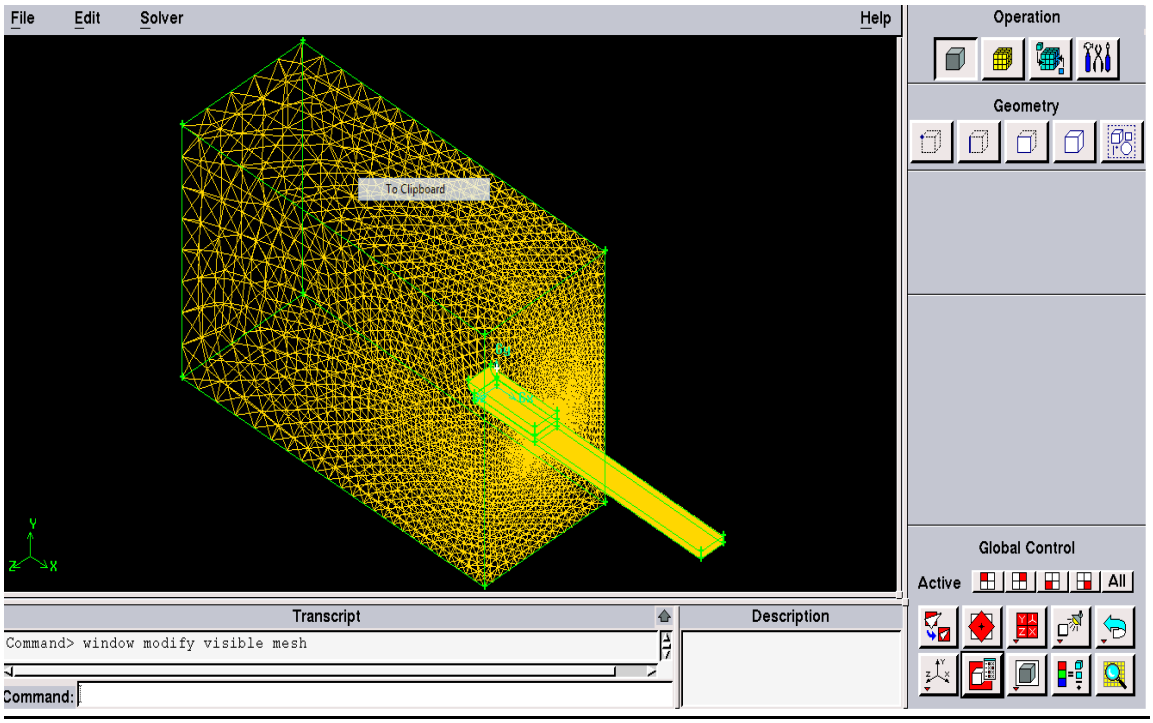

(B)

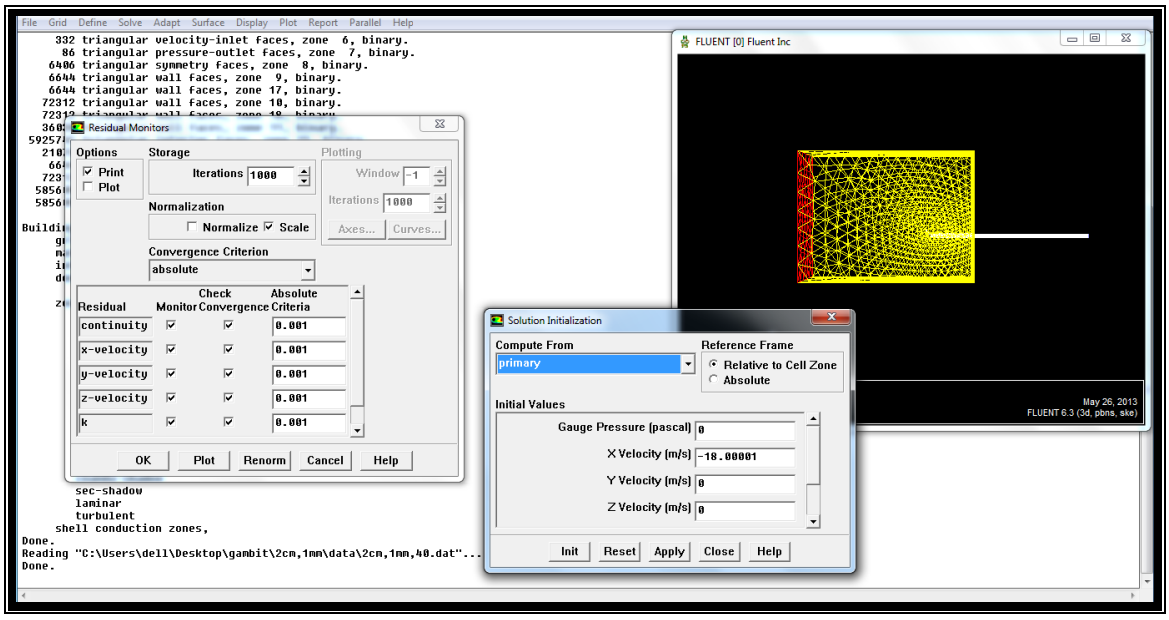

(C)

Figure 3: A-GMBIT software- Specify Boundary Condition.
B- Isometric view for model geometry with mesh.
C- FLUENT software – Solution Monitor &Solution Initialization

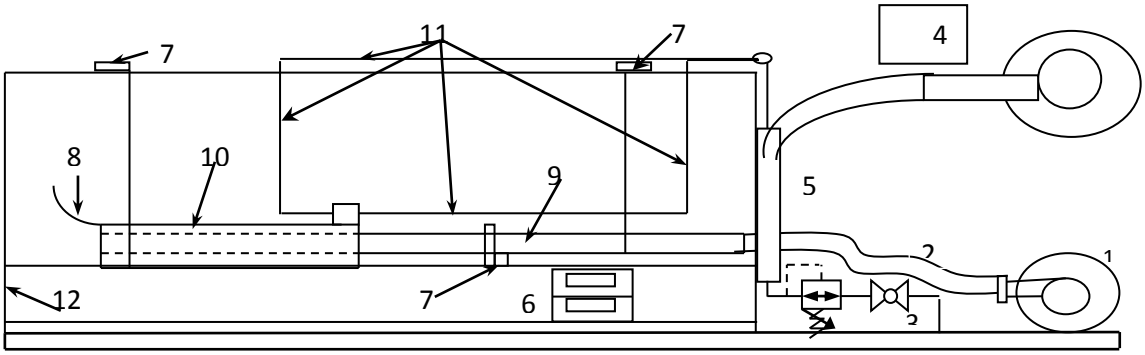

1	Centrifugal Blower	7	four Load Cells
2	Flexible Hose	8	Coanda Surface
3	Ball Valve	9	Main Jet
4	ejector	10	Secondary Jet
5	Flow Meter	11	Pipes
6	Weight Indicator	12	Frame

Figure 4: Schematic of Experimental Rig

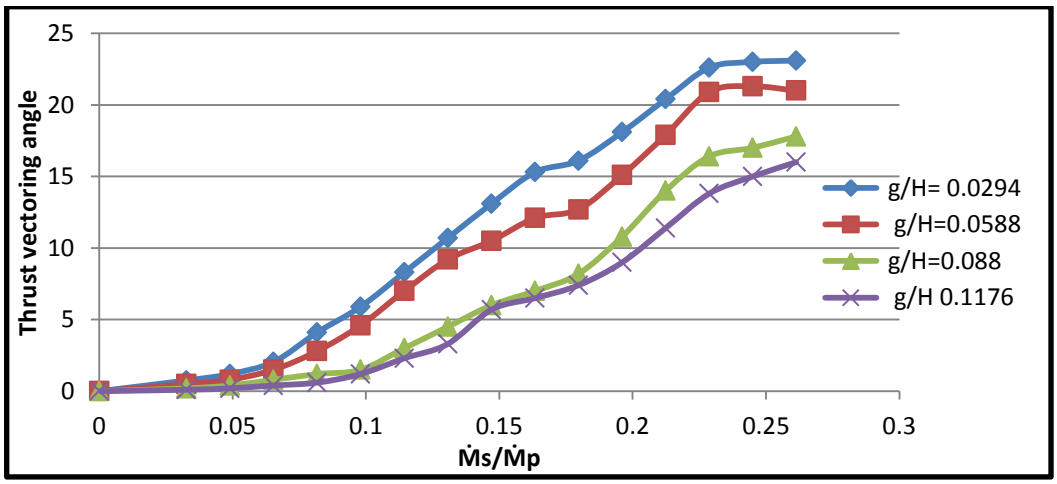

Figure 5: Thrust vectoring angle for varying secondary gap height at constant Coanda surface diameter R/H =1.176

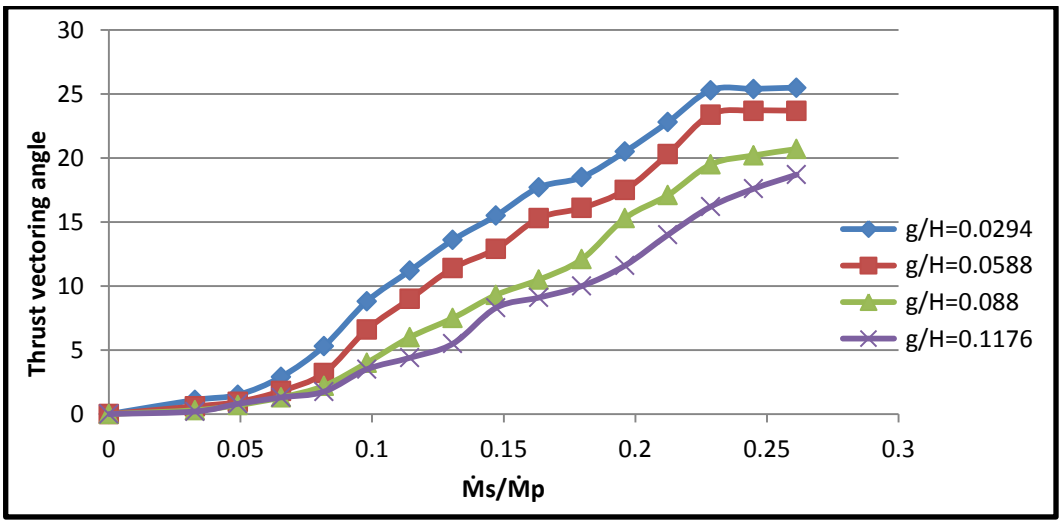

Figure6: Thrust vectoring angle for varying secondary gap height at constant Coanda surface diameter R/H =2.353.

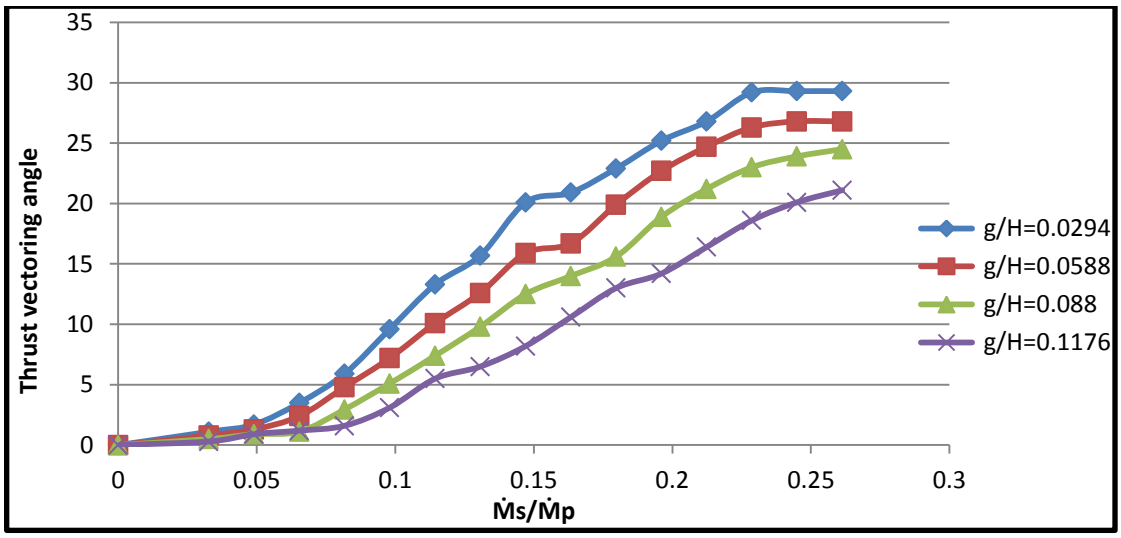

Figure 7: Thrust vectoring angle for varying secondary gap height at constant Coanda surface diameter R/H =3.53.

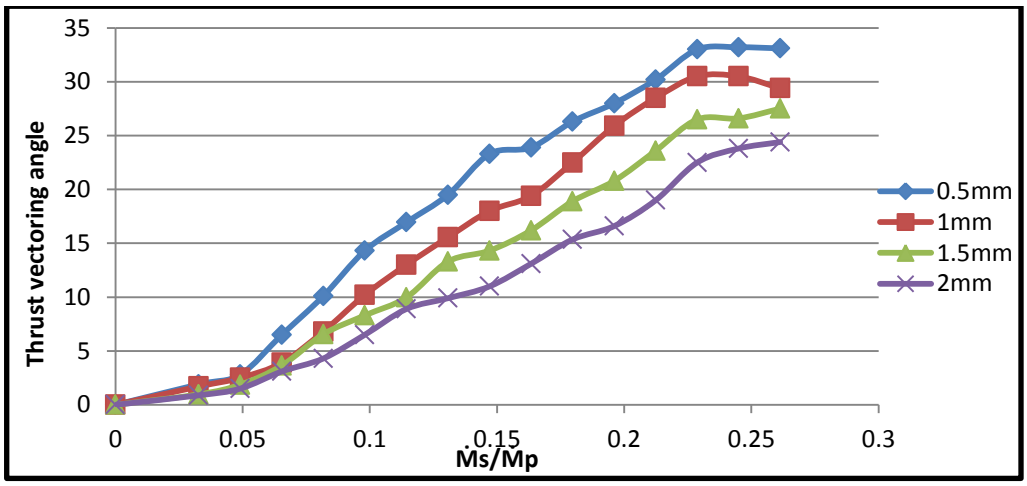

Figure 8: Thrust vectoring angle for varying secondary gap height at constant Coanda surface diameter R/H =4.705.

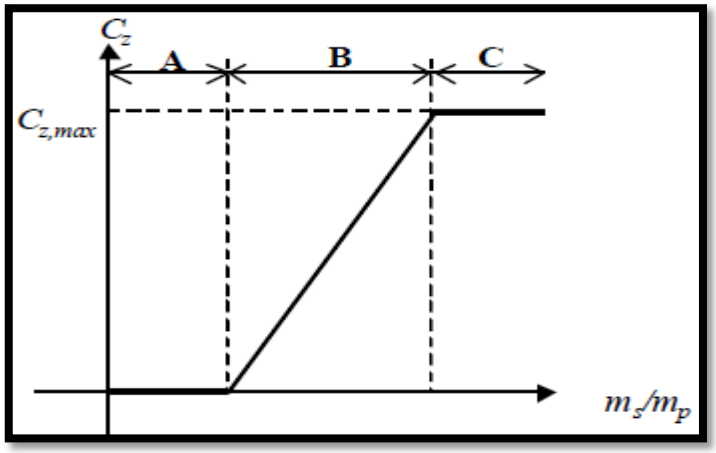

Figure 9: Trend line of the experimental results
A – Dead zone, B – Control, C – Saturation

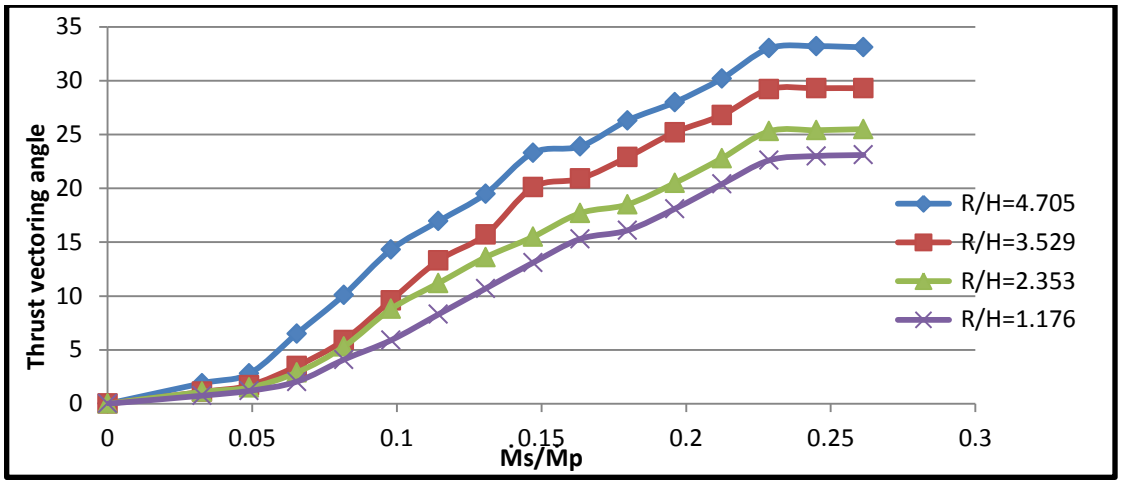

Figure10: Thrust vectoring angle for various Coanda surface diameters at constant secondary gap height g/H=0.0294.

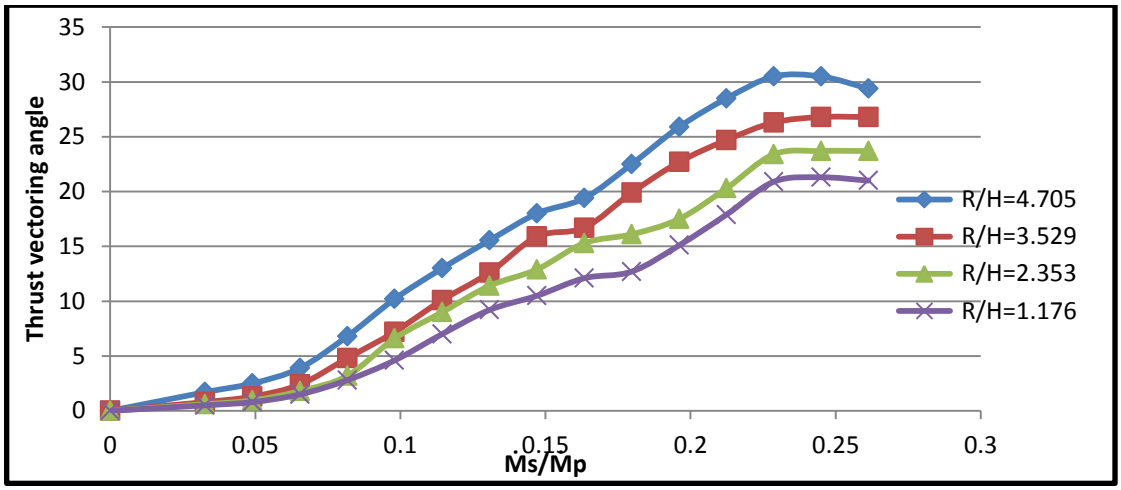

Figure11: Thrust vectoring angle for varying Coanda surface diameters at constant secondary gap height g/H=0.0588.

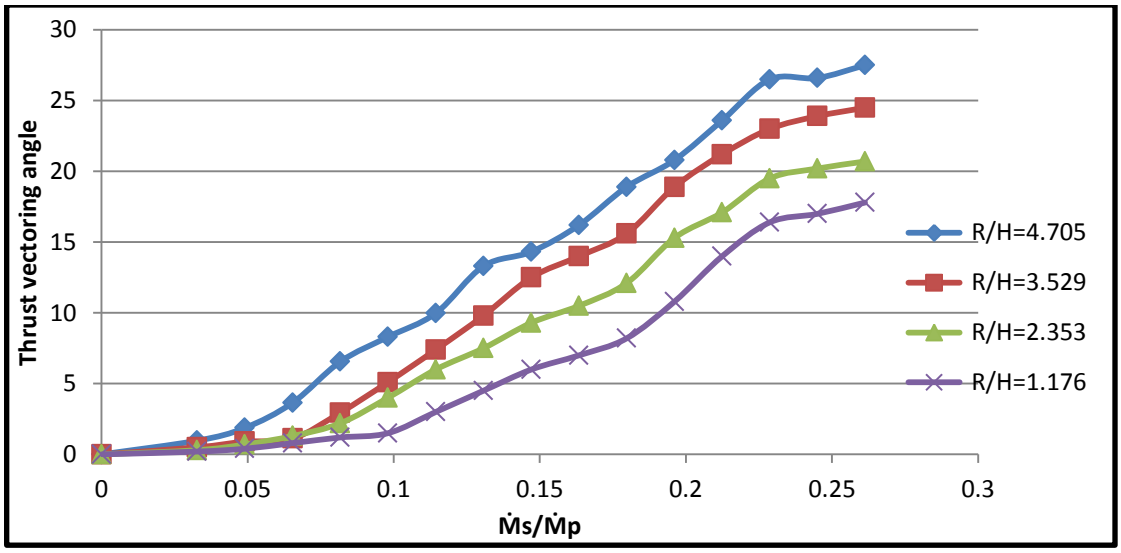

Figure 12: Thrust vectoring angle for varying Coanda surface diameters at constant secondary gap height g/H=0.0882.

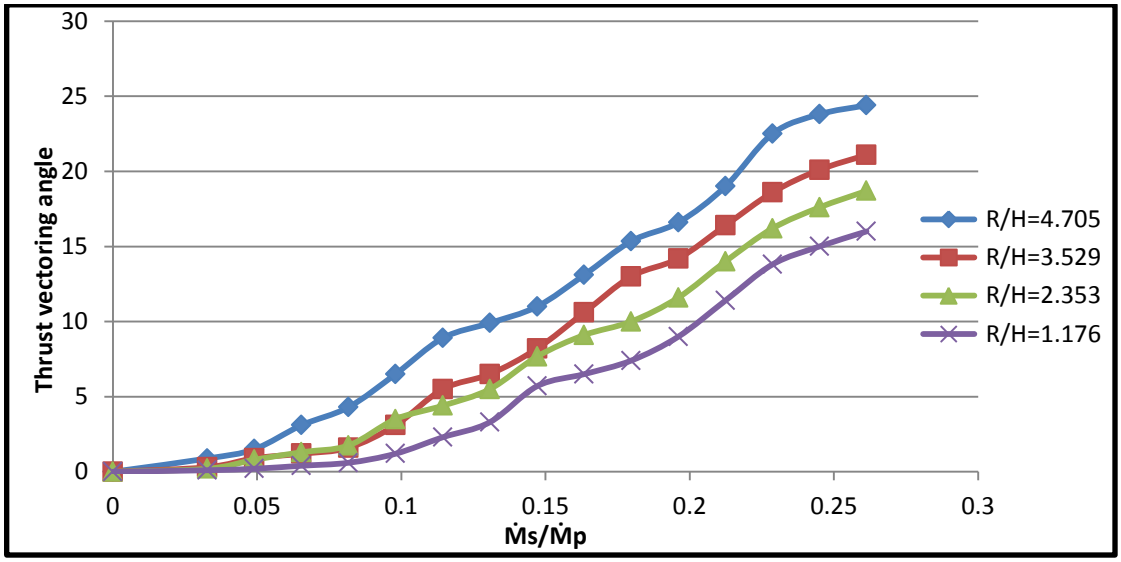

Figure 13: Thrust vectoring angle for varying Coanda surface diameters at constant secondary gap height g/H=0.1176.

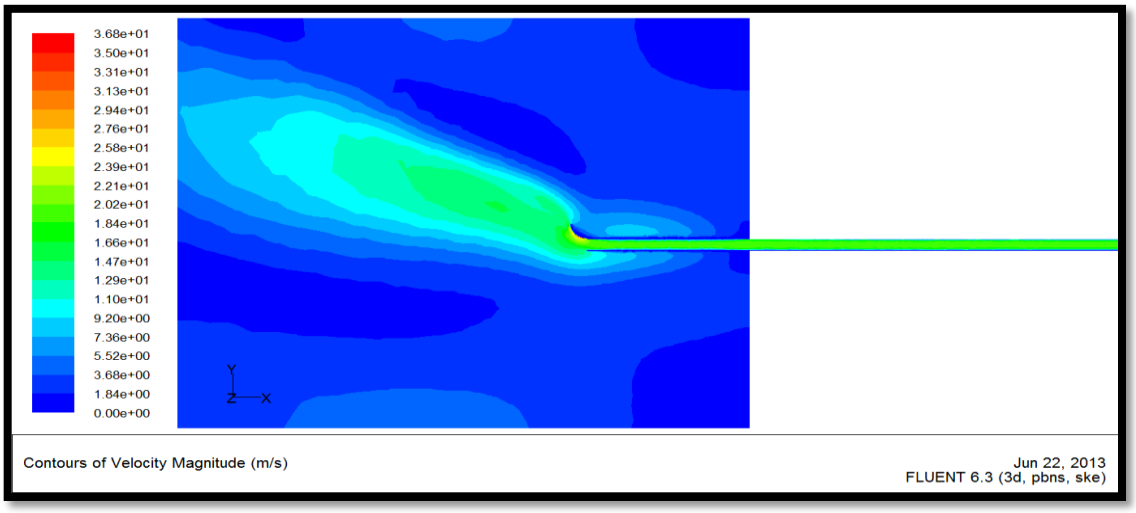

Figure14: Velocity contour at R/H=1.176, g/H = 0.0588 and ms/mp=14.74%.

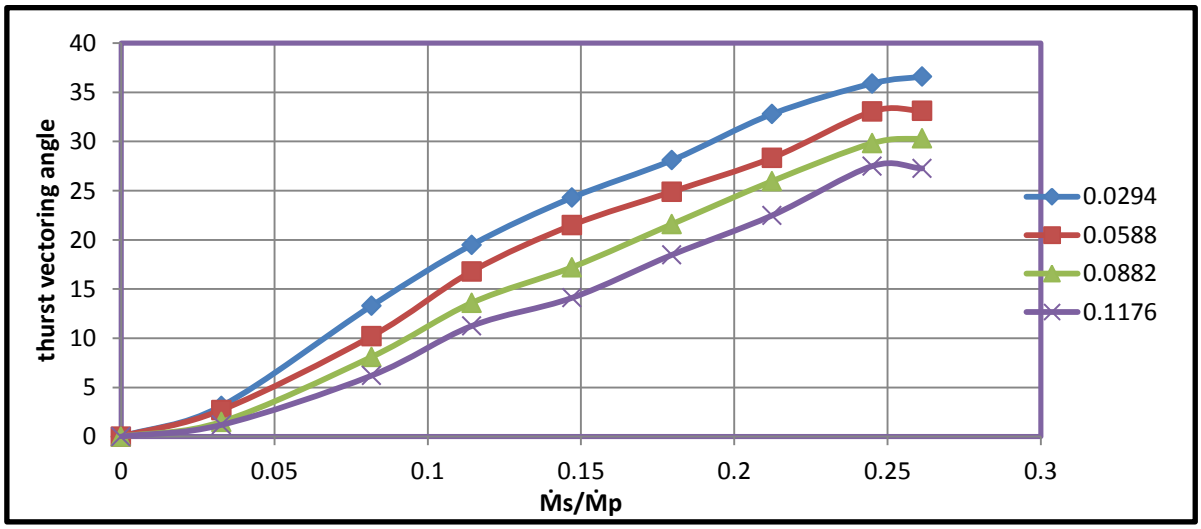

Figure15: Theoretical results of Thrust vectoring angle for varying secondary gap height at constant Coanda surface diameter R/H =4.705 and Vp=18m/s.

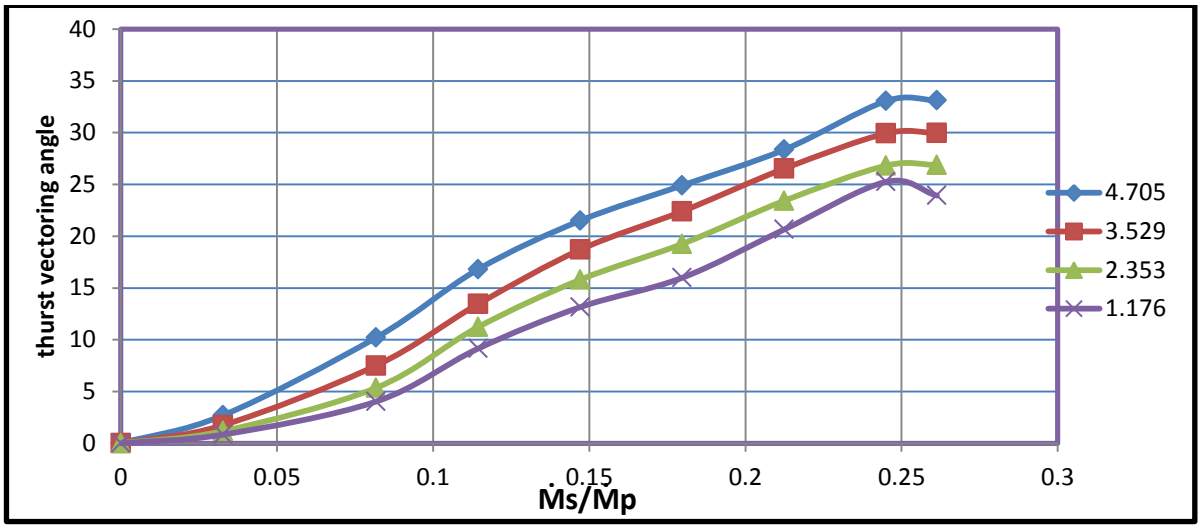

Figure 16: Theoretical results of thrust vectoring angle for varying Coanda at constant secondary gap height g/H=0.0588 and Vp=18m/s.

Figure 17: Visualisation of a non-vectored primary jet for Ms/Mp=0,g/H=2.353.

Figure 18: Visualisation of a vectored primary jet for Ms/Mp=0.2613,g/H=3.53

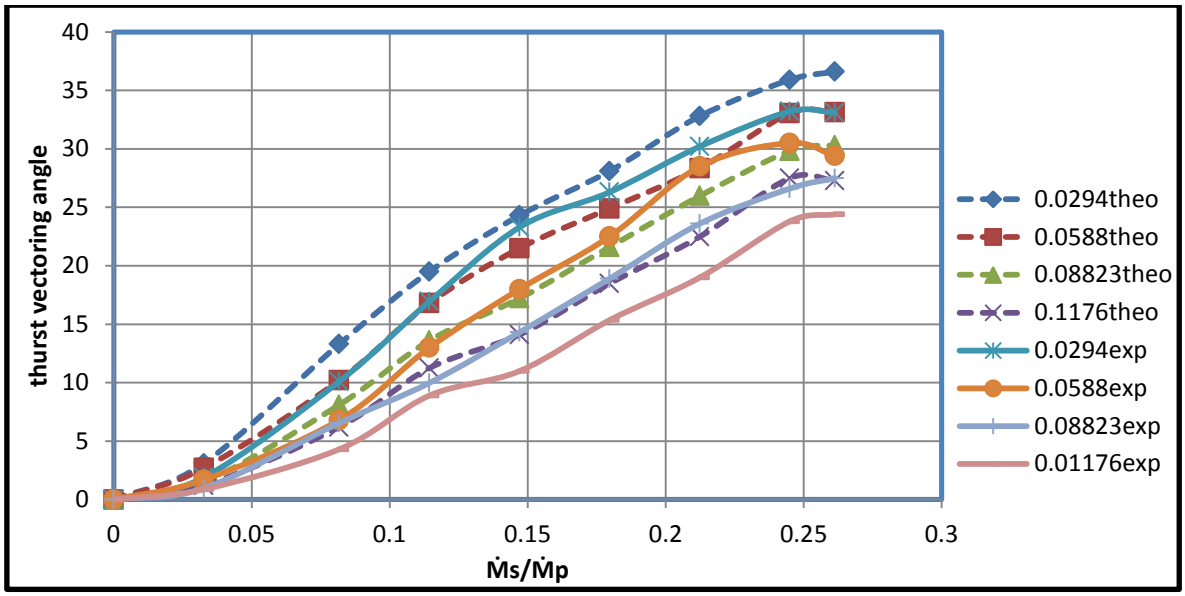

Figure 19: comparison between theoretical and experimental result for varying secondary gap height at constant Coanda surface diameter R/H =4.705 and Vp=18m/s.

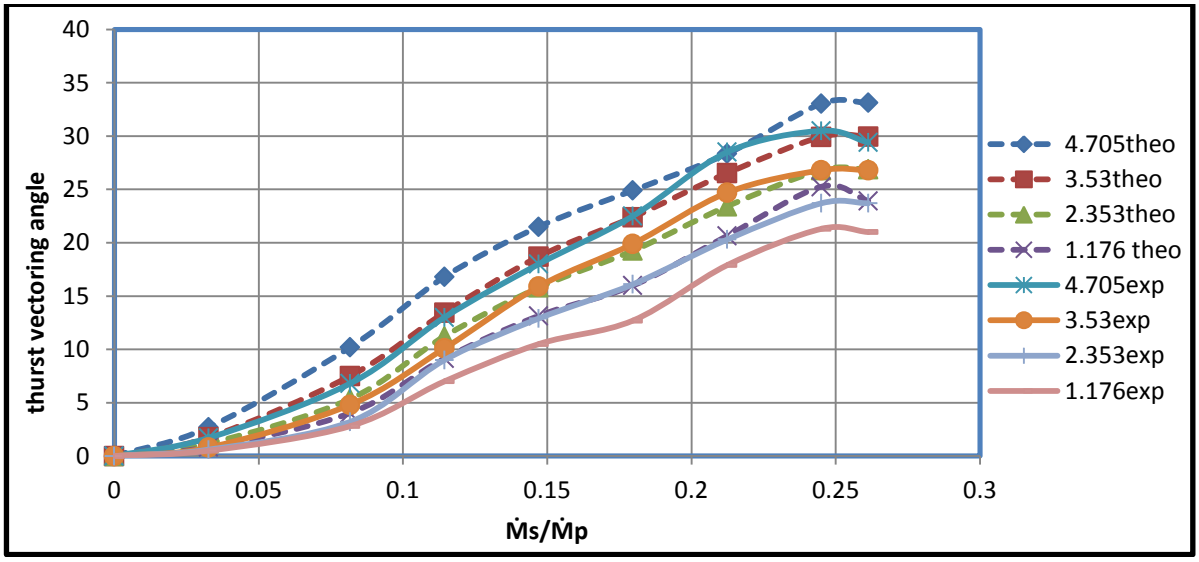

Figure 20: Comparison between theoretical and experimental result for varying Coanda surface diameter at constant secondary gap height g/H=0.0588 and Vp=18m/s.

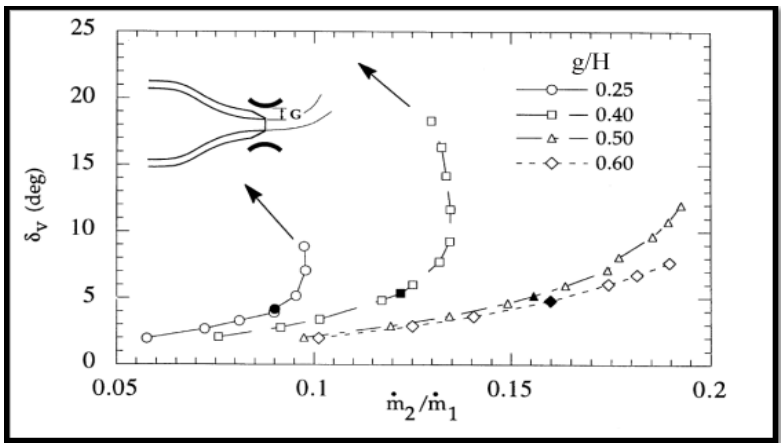

Figure 21: Experimental results [8].

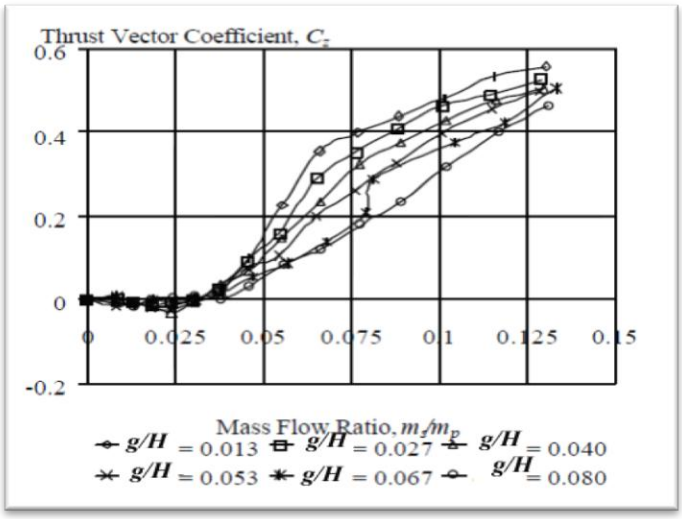

Figure 22: Experimental result [4].

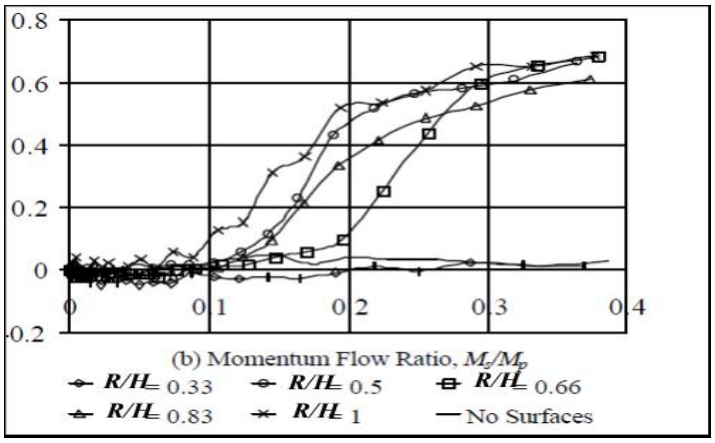

Figure 23: Experimental result [4].

توجيه نفاث مائع دون الصوتي باستخدام طريقة الجريان المعاكس

علي عبد ألمحسن الاسدي
قسم الهندسة الميكانيكية
جامعة بغداد/كلية الهندسة

عمر حسين علي
قسم الهندسة الميكانيكية
جامعة بغداد/كلية الهندس

الخلاصة

تضمن البحث الحالي دراسة عمليه ونظريه لتوجيه نفاث رئيس باستخدام طريقة دفع نفاث ثانوي بالاتجاه المعاكس لاتجاه النفاث الرئيس للاستفادة من ظاهرة (coanda effect) حيث شمل الجانب العملي على تصميم وبناء منظومة كاملة لتوليد النفاث الرئيسي والثانوي حيث أن النفاث الرئيسي على شكل مستطيل (نسبه العرض إلى الارتفاع =4.4) وتم دارسة متغيرات مختلفة على مقدار زاوية انحراف اتجاه النفاث الرئيسي .أن الدراسة العملية تضمنت تغيير نسبة التدفق الكتلي (Ṁs/Ṁp)) اي نسبة التدفق الكتلي للنفاث الثانوي على نسبة التدفق الفعلي للنفاث الرئيسي والذي تراوحت مابين 0≤Ṁs/Ṁp ≤0.31 كذلك تم اخذ أربع ارتفاعات للنفاث الثانوي على ارتفاع النفاث الرئيسي (g/H= (0.0294, 0.0588, 0.088, 0.1176 وتم اخذ أربع أقطار .(R/H= (1.176, 2.353, 3.529 and 4.705 أما بالنسبة للجانب النظري فتم عمل محاكاة باستخدام Fluent 6.3.26 لغرض التحليل النظري لبعض الحالات العملية. من البحث تم الحصول على توجيه كامل للنفاث الرئيسي باستخدام نفاث ثانوي وبينت التجارب العملي تطابق جيد مع النتائج النظرية حيث لوحظ ان النتائج تحتوي على ثلاث مناطق المنطقة الأولى والتي تسمى dead zone والذي ينعدم فيها التوجيه ومنطقة التوجيه control zone ومنطقة ثالثة هي Saturation zone الذي فيها يثبت مقدار التوجه وأثبتت ان بزيادة معدل التدفق الثانوي إلى الرئيسي إلى زيادة مقدار زاوية انحراف النفاث وان وقطر السطح المنحني (coanda surface) يحدد مدى منطقة انعدام التوجيه , (dead zone) كما لوحظ ان ارتفاع فتحة النفاث الثانوي لها علاقة عكسية مع مقدار زاوية انحراف النفاث. وتم مقرنة نتائج البحث الحالي مع بحوث سابقه وقد أظهرت تماثل جيد. رقم ماخ أقل من 0.5.

الكلمات المفتاحية: زاوية توجيه دفع نفاث؛ توجيه نفاث؛ ظاهرة السطح المنحنى؛ الجريان المتعاكس؛ معدل التدفق الكتلي.